

OPTIMIZED TRAJECTORIES TO THE NEAREST STARS USING LIGHTWEIGHT HIGH-VELOCITY PHOTON SAILS

RENÉ HELLER,¹ MICHAEL HIPPKKE,² AND PIERRE KERVELLA^{3,4}

¹*Max Planck Institute for Solar System Research, Justus-von-Liebig-Weg 3, 37077 Göttingen, Germany*

²*Lwiter Straße 21b, 47506 Neukirchen-Vluyn, Germany*

³*Unidad Mixta Internacional Franco-Chilena de Astronomía, CNRS/INSU UMI 3386 and Departamento de Astronomía, Universidad de Chile, Casilla 36-D, Santiago, Chile*

⁴*LESIA (UMR 8109), Observatoire de Paris, PSL Research University, CNRS, Sorbonne Universités, UPMC Univ. Paris 06, Univ. Paris Diderot, Sorbonne Paris Cité, 5 Place Jules Janssen, 92195 Meudon, France*

ABSTRACT

New means of interstellar travel are now being considered by various research teams, assuming lightweight spaceships to be accelerated via either laser or solar radiation to a significant fraction of the speed of light (c). We recently showed that gravitational assists can be combined with the stellar photon pressure to decelerate an incoming lightsail from Earth and fling it around a star or bring it to rest. Here, we demonstrate that photogravitational assists are more effective when the star is used as a bumper (i.e. the sail passes “in front of” the star) rather than as a catapult (i.e. the sail passes “behind” or “around” the star). This increases the maximum deceleration at α Cen A and B and reduces the travel time of a nominal graphene-class sail (mass-to-surface ratio 8.6×10^{-4} gram m^{-2}) from 95 to 75 yr. The maximum possible velocity reduction upon arrival depends on the required deflection angle from α Cen A to B and therefore on the binary’s orbital phase. Here, we calculate the variation of the minimum travel times from Earth into a bound orbit around Proxima for the next 300 yr and then extend our calculations to roughly 22,000 stars within about 300 ly. Although α Cen is the most nearby star system, we find that Sirius A offers the shortest possible travel times into a bound orbit: 69 yr assuming 12.5% c can be obtained at departure from the solar system. Sirius A thus offers the opportunity of flyby exploration plus deceleration into a bound orbit of the companion white dwarf after relatively short times of interstellar travel.

Keywords: radiation mechanisms: general — solar neighborhood — space vehicles — stars: kinematics and dynamics — stars: individual (α Centauri, Sirius)

heller@mps.mpg.de

hippke@ifda.eu

pierre.kervella@obspm.fr

1. INTRODUCTION

The possibility of interstellar travel has recently been revived through developments in laser technology, material sciences, and the construction of high-performance nano computer chips (Lubin 2016; Manchester & Loeb 2017). The small weight of only a few grams of on-board equipment (communication, navigation, propulsion, science instruments, etc.) and the possible mass production of these probes results in reduced costs for production, launch, and operation – benefits that could make such a mission affordable within the current century.¹ Moreover, the first interplanetary solar sail mission (IKAROS; Tsuda et al. 2011) has been completed and further concepts are now being tested in near-Earth orbits (e.g. LightSail; Ridenoure et al. 2016).

The idea of using solar light to accelerate a space probe in the solar system is not new (Kepler 1619; Tsander 1924; Tsiolkovskiy 1936; Garwin 1958; Tsu 1959). Key challenges are in the high temperatures close to the sun, where the thrust is strongest but the sail could melt (Dachwald 2005), and in the loss of effective propulsion at several AU from the Sun. Using a close (0.1 AU) solar encounter and a 1000 m radius sail, Matloff et al. (2008) calculated a maximum velocity of 0.2% c for the departure of a 150 kg probe from the solar system. Alternatively, it has been proposed that lasers could solve the decreasing-strength-with-distance problem due to their high flux of coherent light (Forward 1962; Marx 1966). As noted by Redding (1967), however, this launch technology meets the problem of deceleration at the destination since there would be no obvious way to decelerate the spacecraft at the target star.

Heller & Hippke (2017) suggested to decelerate and deflect incoming high-velocity sails from Earth using the stellar radiation and gravitation, a maneuver they referred to as photogravitational assist. Assuming that the sail would be made of a strong, ultralight material such as graphene, which would be covered by a highly reflective broadband coating made of sub-wavelength thin metamaterials (Slovick et al. 2013; Moitra et al. 2014), such a sail could have a maximum speed at arrival ($v_{\infty, \max}$) of about 4.6% c to be successively decelerated at the stellar triple α Cen A, B, and C (Proxima) (Matloff 2013). Such a tour could potentially park the lightsail in a bound orbit around the Earth-mass habitable zone exoplanet Proxima b (Anglada-Escudé et al. 2016). The travel times would be 95 yr from Earth to α Cen AB and another 46 yr from the AB binary to Proxima, or 141 yr in total.

Here, we present an alternative way of using photogravitational assists at α Cen, which reduces travel times significantly. We also present a detailed analysis of

the AB orbital motion for the next three centuries, which is crucial for a detailed study of the expected travel times at a given launch time from the solar system. We then apply this method to stars within 300 ly of the sun and identify other highly interesting targets for bound-orbit exploration by interstellar lightsails.

2. METHODS

2.1. A Nominal Graphene-class Sail

In our nominal scenario, we consider a sail made of a graphene structure ($\sigma = 7.6 \times 10^{-4}$ gram m^{-2}) with a graphene-based rigid skeleton and highly reflective coating that is capable of transporting a science payload (laser communication, navigation, cameras, etc.) of about 1 gram (Heller & Hippke 2017). Such a sail must have an area of about $10^5 m^2 = (316 m)^2$ to make the weight of the science payload negligible against the weight of the sail structure. At this size, the graphene structure would contribute 76 gram, the skeleton and coating could add 9 gram, and the payload would add another 1 gram, implying $\sigma_{\text{nom}} = 8.6 \times 10^{-4}$ gram m^{-2} for our nominal graphene-class sail.

2.2. Photogravitational Assists at α Cen

2.2.1. An Improved Method for Deceleration

In Heller & Hippke (2017), we showed how it is possible to use both the photon pressure of a star and its gravitational tug to decelerate and deflect an incoming lightsail. Our main aim was to determine the maximum possible injection speed ($v_{\infty, \max}$) at α Cen A to allow a swing-by maneuver to α Cen B and to finally achieve a bound orbit around Proxima. The key challenge that we identified for the determination of $v_{\infty, \max}$ is in reaching the maximum deceleration upon arrival at α Cen A while simultaneously achieving the required deflection angle (δ) between the inbound and outbound trajectories in order to swing from α Cen A to B. Analytical estimates for our nominal graphene-class sail, which would approach the star as close as five stellar radii (R_{\star}), show that it could be possible to drop as much as 12,900 $km s^{-1}$ at A, 8800 $km s^{-1}$ at B, and another 1270 $km s^{-1}$ at Proxima, giving an additive deceleration of up to $v_{\infty, \max} = 22,970 km s^{-1}$ in total.

We then performed numerical calculations using a modified N -body code that included the forces on the sail imposed by the stellar photon pressure. We imposed an analytic boundary condition on the sail's pitch angle (α , the angle between the normal to the sail plane and the radius vector to the star) to maximize the loss of speed along its trajectory. In our simulations, the sail was inserted into the gravitational well of the star in such a way that it would pass the star on the one side (e.g. on the right, see Fig. 2 in Heller & Hippke 2017) and have a net deflection after its passage to the other side (e.g. to the left).

¹ See the Breakthrough Starshot Initiative at <http://breakthroughinitiatives.org>

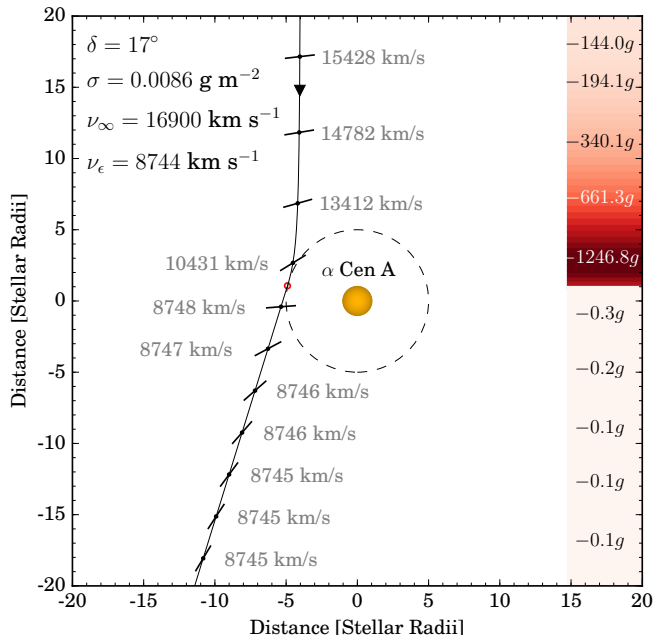


Figure 1. Trajectory of a lightsail performing a photogravitational assist at α Cen A (orange circle). The bars along the trajectory visualize the instantaneous orientation of the sail (in steps of 60 min) determined to maximize the deceleration. The values in the legend denote the deflection angle, the mass-to-surface ratio, the inbound velocity, and the outbound velocity of the sail. The color bar at the right shows the g -forces acting on the sail along the trajectory, where $g = 9.81 \text{ m s}^{-2}$ is the acceleration on the Earth’s surface.

These numerical simulations revealed that the maximum velocity upon arrival at A, which would allow a deflection to B (assuming $\delta \approx 10^\circ$), is limited to $v_{\infty, \text{max}} = 13,800 \text{ km s}^{-1}$. And so while analytical estimates of the additive nature of the photogravitational assist suggest that up to $v_{\infty, \text{max}} = 22,970 \text{ km s}^{-1}$ could be successively absorbed at the α Cen stellar triple, numerical simulations show that the particular geometry of the system limits $v_{\infty, \text{max}}$ to $13,800 \text{ km s}^{-1}$.

Following up on these simulations, we recently discovered that a simple modification of the incoming trajectory yields higher deflection angles at even higher incoming speeds. It turns out that it is more effective to use the stellar photon pressure (rather than gravity) to enhance the deflection. From a geometry perspective, it is more efficient to let the sail approach the star on the same side (e.g. on the left; see Figure 1) as the desired deflection (i.e. to the left). We then find that, using the same optimization strategy for deceleration as Heller & Hippke (2017), a maximum total deceleration of $v_{\infty, \text{max}} = 17,050 \text{ km s}^{-1}$ can be reached at $\delta = 19^\circ$, where 8800 km s^{-1} and 8400 km s^{-1} can be lost at A and B, respectively. If the lightsail is supposed to continue its journey on to Proxima, then it would actually be better to orient the sail during its passage at

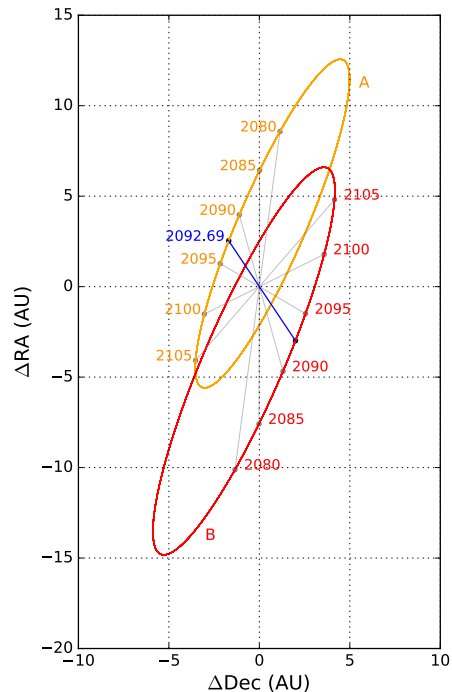


Figure 2. Orbital trajectories of α Cen A (orange) and B (red) in their barycentric coordinate system as seen from Earth using differential R.A. and decl. coordinates. The AB vector at the time of their closest apparent encounter in 2092.69 (8 September 2092) is marked in blue.

B in a way to avoid maximum deceleration, so that the sail can continue its cruise to Proxima with a residual speed of 1270 km s^{-1} . This is the maximum speed that can ultimately be absorbed at Proxima.

2.2.2. A Timetable of Launch Opportunities to Proxima

The orbital motion of the α Cen AB binary leads to a periodic variation ($P = 79.929 \pm 0.013 \text{ yr}$; Kervella et al. 2016) of the deflection at α Cen A that is required by the sail to reach B. We calculate the binary’s orbital motion for the next 300 yr, based on the works of Kervella et al. (2016), and we include the computation of Proxima’s orbit around the α Cen AB binary based on Kervella et al. (2017b). Figure 2 shows the orbits of α Cen A (orange) and B (red) as a projection on the sky with dates around the year 2100 labeled along the ellipses. The blue line illustrates the sky-projected AB vector at the time when the deflection required by the sail for a sequential AB photogravitational assist is smallest. This event will take place on 8 September 2092 (2092.69).

We then use our results for $\delta(t)$, where t symbolizes time, together with a range of numerical trajectory simulations, to first determine $v_{\infty, \text{max}}(\delta)$, then $v_{\infty, \text{max}}(t)$, that is, the maximum possible injection speed at α Cen to reach a bound orbit at Proxima, and ultimately the travel time from Earth to α Cen AB over the next 300 yr. For the final step, the conversion from travel speed to

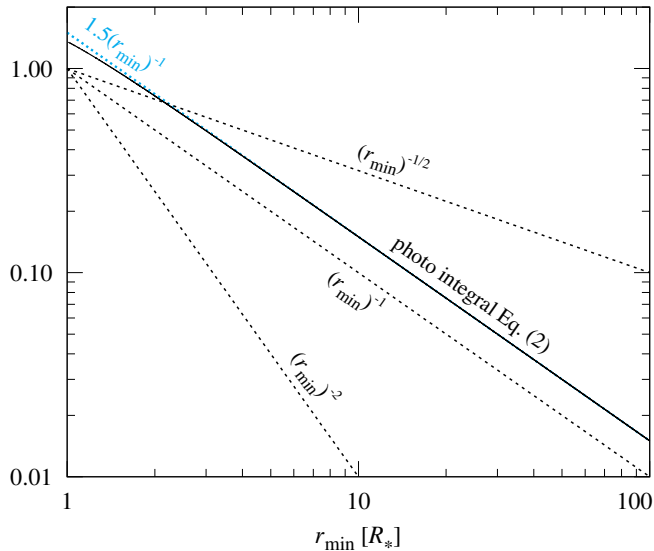


Figure 3. Integral in Equation (2) as a function of r_{\min} , the closest stellar encounter (solid line). Our nominal calculations invoke a sail approaching as close as $r_{\min} = 5 R_{\star}$, where the integral amounts to 0.299. Four different functions are shown for comparison (dotted lines). Note that $1.5/r_{\min}$ provides an exquisite fit (blue dotted line), e.g. $1.5/5 = 0.3$.

travel time, we adopt a barycentric distance to α Cen AB of 4.365 ly (Kervella et al. 2016).

2.3. An Interstellar Travel Catalog

2.3.1. Analytical Estimates

While the α Cen system is the natural first target for interstellar travels to consider, given its proximity and the presence of the Earth-sized, potentially habitable planet Proxima b, other nearby stars offer compelling opportunities, too. We thus extend our investigations of photogravitational assists to a full stop around other nearby stars and estimate the travel time (τ) to a nearby star with a given radius (R_{\star}) and luminosity (L_{\star}) as

$$\tau = \frac{d}{v_{\infty, \max}} = \frac{d}{\sqrt{\frac{2E_{\text{kin}}}{M}}}, \quad (1)$$

where d is the stellar distance to the Sun, M is the sail mass,

$$\begin{aligned} E_{\text{kin,p}} &= \int_{r_{\min}}^{\infty} dr F(r) \\ &= \frac{L_{\star} A}{3\pi c R_{\star}} \int_{r_{\min}}^{\infty} dr \left(\left[1 - \left[1 - \left(\frac{R_{\star}}{r} \right)^2 \right]^{3/2} \right] \frac{1}{R_{\star}} \right) \end{aligned} \quad (2)$$

is the kinetic energy of the sail that can be absorbed by the stellar photons during approach (McInnes & Brown 1990; Heller & Hippke 2017), and A is the sail's surface

area. The integral in Equation (2), which we refer to as the photointegral, is independent of the actual value of R_{\star} and only depends on the choice of r_{\min} . Figure 3 shows the numerical value of the photointegral for $1 R_{\star} \leq r_{\min} \leq 100 R_{\star}$. Four different functions are given for comparison (dotted lines). In particular, we found that $1.5/r_{\min}$ (with r_{\min} in units of R_{\star}) provides an excellent approximation with deviations $< 1\%$ for $r_{\min} \geq 3 R_{\star}$ (blue dotted line). Using this approximation, Equation (2) becomes

$$E_{\text{kin,p}} = \frac{L_{\star} A}{2\pi c R_{\star} (r_{\min}/R_{\star})} = \frac{L_{\star} A}{2\pi c r_{\min}} \quad (3)$$

and Equation (1) then is equivalent to

$$\begin{aligned} \tau &= \frac{d}{\sqrt{\frac{L_{\star} A}{\pi c r_{\min} M}}} \\ \Leftrightarrow \log_{10}(\tau(\text{yr})) &= \frac{1}{\ln(10)} \ln \left(\frac{d/\text{yr}}{\sqrt{\frac{L_{\star} A}{\pi c r_{\min} M}}} \right) \end{aligned} \quad (4)$$

We chose the latter equivalent transformation to describe the travel time as a logarithmic spiral of the form $\varphi(d) = 1/k \ln(d/a)$, where the constant $k > 0$ defines the curvature of the spiral and a is the radius of the circle for $k \rightarrow 0$. As an aside, note that the first line in Equation (6) is equivalent to $\tau \propto \sigma$, a relation that we will come back to below.

For a nominal minimum stellar approach of $r_{\min} = 5 R_{\star}$, the photointegral yields a value of 0.299 and Equation (2) collapses to

$$E_{\text{kin,p}} = \frac{L_{\star} A}{10\pi c R_{\star}}, \quad \text{for } r_{\min} = 5 R_{\star}. \quad (5)$$

so that

$$\log_{10}(\tau(\text{yr})) = \frac{1}{\ln(10)} \ln \left(\frac{d/\text{yr}}{\sqrt{\frac{L_{\star} A}{5\pi c R_{\star} M}}} \right) \quad (6)$$

2.3.2. Numerical Simulations

In addition to our analytical estimates, we perform numerical simulations of photogravitational assists around stars in the solar neighborhood as in Heller & Hippke (2017). For 117 stars within 21 ly around the Sun, we use distances, luminosities, masses and radii from Allende Prieto et al. (2004), Valenti & Fischer (2005), van Leeuwen (2007), and Holmberg et al. (2009).²

² For an extensive list of references, see <http://www.johnstonsarchive.net/astro/nearstar.html>

For more distant stars but within 316 ly, we use parallax measurements from Hipparcos (Perryman et al. 1997) and Gaia DR1 (Gaia Collaboration et al. 2016a,b; Lindegren et al. 2016) to estimate stellar distances. We pull available estimated temperatures from the Radial Velocity Experiment (RAVE) (Casey et al. 2017; Kunder et al. 2017) and add additional stars from the Hipparcos and Tycho-2 catalog (Høg et al. 2000), where only color information ($B - V$) is available. For these latter stars, we follow the procedure of Heller et al. (2009) to estimate the effective temperature as

$$T_{\text{eff}} = 10^{[14.551 - (B - V)]/3.684} \text{ K} , \quad (7)$$

the stellar radius R_* as

$$\frac{R_*}{R_\odot} = \left[\left(\frac{5770 \text{ K}}{T_{\text{eff}}} \right)^4 10^{(4.83 - M_V)/2.5} \right]^{1/2} , \quad (8)$$

and the stellar mass M_* as

$$\frac{M_*}{M_\odot} = \left(\frac{4\pi R_*^2 \sigma_{\text{SB}} T_{\text{eff}}^4}{L_\odot} \right)^{1/\beta} , \quad (9)$$

where σ_{SB} is the Stefan-Boltzmann constant and where the coefficient β in the relation $L \propto M^\beta$ depends on the stellar mass (see Table 1; values taken from Cester et al. 1983).

Table 1. Empirical Values for β in the Mass-Luminosity Relation.

β	Stellar Mass
3.05 ± 0.14	$M_* \lesssim 0.5 M_\odot$
4.76 ± 0.01	$0.6 M_\odot \lesssim M_* \lesssim 1.5 M_\odot$
3.68 ± 0.05	$1.5 M_\odot \lesssim M_*$

In our modified N -body simulations, we impose an upper temperature (T) limit of 100°C (373 K) on the sail. At these temperatures, modern silicon semiconductors are still operational (Intel Corporation 2016) and the sail material is likely not a limitation. For comparison, aluminum has a melting point of 933 K, and graphene melts at 4510 K (Los et al. 2015).

We assume a sail reflectivity of 99.99%, which might be achievable in the broadband using multiple coatings, or metamaterials with sub-wavelength thickness (Slovick et al. 2013; Moitra et al. 2014; Liu et al. 2016). From the Boltzmann law, we first deduce

$$T_{\text{eff}} < T \times (n^2/\zeta)^{1/4} , \quad (10)$$

where $\zeta = (1 - 0.9999)$ is the absorptivity of the sail and $n = r_{\text{min}}/R_*$, and then we calculate

$$n = \sqrt{\zeta} \times (T_{\text{eff}}/T)^2 \quad (11)$$

as the minimum (float) number of stellar radii for the sail to prevent heating above $T = 373 \text{ K}$. As an example, for Sirius A ($T_{\text{eff}} = 8860 \text{ K}$) we obtain $n = \sqrt{1 - 0.9999} \times (8860/373)^2 = 5.6$ (stellar radii) as a minimum distance. For stars with $T_{\text{eff}} < 8340 \text{ K}$ we have $n < 5$ and so we impose $n = 5$ to limit the destructive perils of flares, magnetic fields, electron/proton impacts, etc.

3. RESULTS

3.1. Optimized Trajectories to Proxima

Using photogravitational assists at the same side of the star as the desired deflection (see Figure 1) rather than gravitational swing-bys “behind” the star (as in Heller & Hippke 2017), we find that the maximum possible injection speed at $\alpha \text{ Cen A}$ to allow deflections to B and then to C can be significantly increased. For a nominal graphene-class lightsail with a mass-to-surface ratio of $\sigma_{\text{nom}} = 10 \times 8.6 \text{ gram m}^{-2}$, we find $v_{\infty, \text{max}} = 17,050 \text{ km s}^{-1}$ (5.7% c). Compared to the previously published value of $v_{\infty, \text{max}} = 13,800 \text{ km s}^{-1}$ (4.6% c , Heller & Hippke 2017), this corresponds to an increase of 24% in speed and implies a reduction of the travel time from Earth to $\alpha \text{ Cen AB}$ from 95 yr to 75 yr. The total travel time from Earth to a full stop at Proxima then becomes 75 yr + 46 yr = 121 yr, assuming a residual velocity of 1280 km s^{-1} can be absorbed at Proxima after 46 yr of travel between $\alpha \text{ Cen B}$ and Proxima.

In Figure 4, we present our results for the variation of the total travel time to Proxima over the next 300 yr. The upper left panel shows the deflection angle required by the sail upon passage of $\alpha \text{ Cen A}$ to reach B. The minimum value is 10.7° .

In the top right panel, we show the maximum possible injection speed at A that allows deflection by an angle δ . The peak velocity of $17,050 \text{ km s}^{-1}$ occurs at an angle of 19° . The shaded regions in the panel denote angles smaller (or larger) than the smallest (or largest) angular separation between A and B, which are thus irrelevant for real trajectories.

The bottom left panel shows the variation of the total travel time from Earth to $\alpha \text{ Cen A}$ given our knowledge about the upcoming orbital alignments (top left panel) and the possible maximum injection speeds (top right panel). The pairs of depressions, e.g. near the departure years 2093 and 2106, correspond to phases of close alignments between A and B, with the first depression referring to an A–B sequence and the second depression corresponding to a B–A sequence, where B is visited first and A thereafter (since A in this case is behind B, as seen from Earth).

The bottom right panel, finally, shows the year of arrival given a year of departure and assuming maximum injection speeds at the time of arrival. As a bottom line of this analysis, we find that the minimum travel time of a graphene-class lightsail from Earth to the $\alpha \text{ Cen AB}$

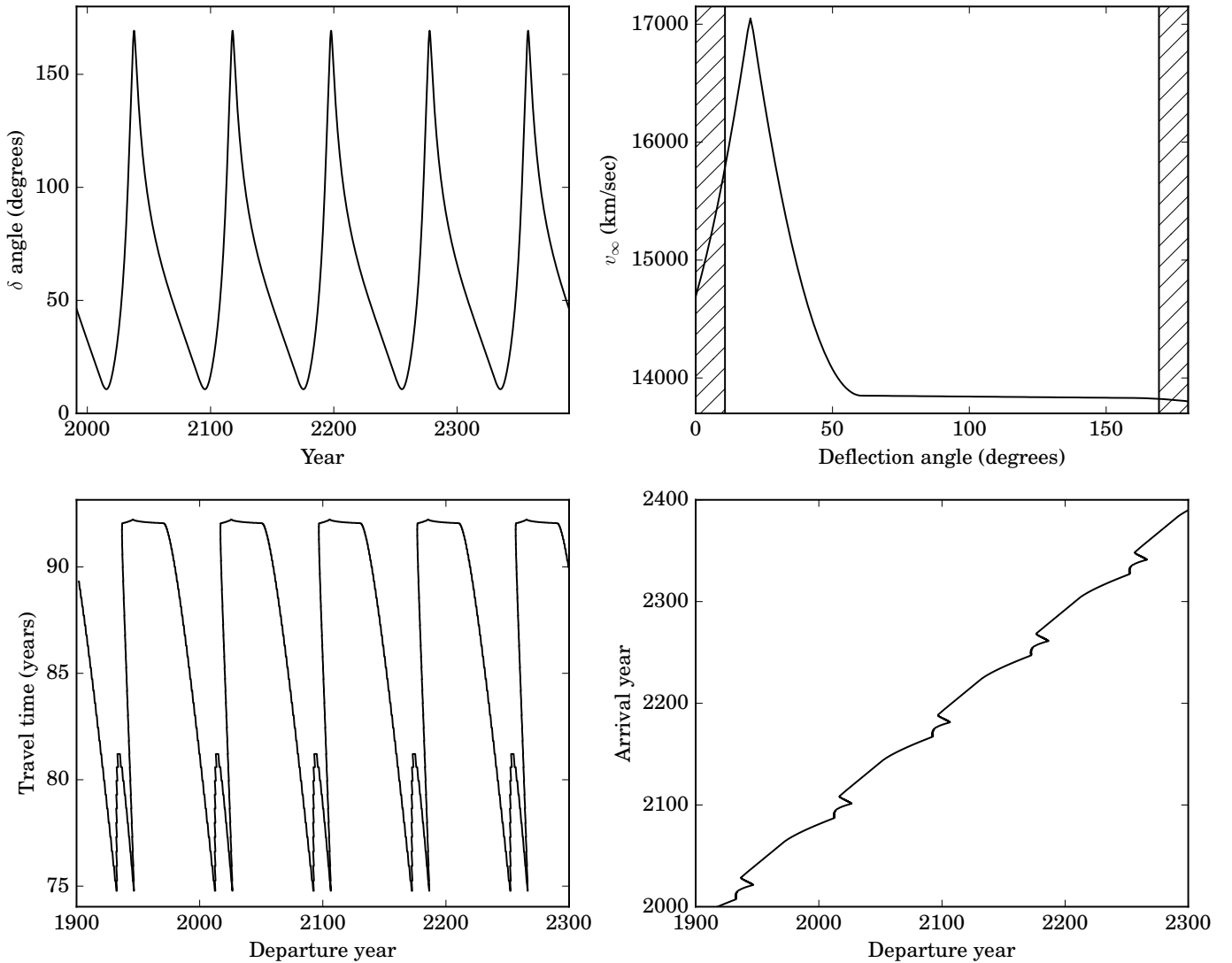


Figure 4. Deflection angles between α Cen A and B and maximum injection speeds at α Cen required by a nominal lightsail made of graphene to perform photogravitational assists into a bound orbit around Proxima. Values have been determined by numerical trajectory simulations with minimum stellar approaches of $5 R_\star$ around either α Cen A or B, whichever was closer to Earth at the time of arrival. *Top left:* Temporal variation of the angular deflection required upon arrival at α Cen to either reach B after the encounter with A or to reach A after encounter with B. *Top right:* Maximum possible injection speed at α Cen A to achieve a given deflection angle. The maximum speed can be obtained for $\delta = 19^\circ$. *Bottom left:* Year of departure from Earth versus travel time between Earth and α Cen AB. The pairs of depressions correspond to maximum injection speeds of $17,050 \text{ km s}^{-1}$ at angular separations of 19° (see upper right panel), which occur a few years before and after the closest encounter of the α Cen AB binary. *Bottom right:* Arrival time at α Cen AB as a function of departure time from Earth.

binary varies between about 75 yr and 95 yr. These values will reduce by a factor of about 3/4 over the next roughly 30,000 yr as the α Cen system approaches the Sun from a bit more than 4 ly today to a minimum separation of about 3 ly.

In Figure 5, we extend our study and investigate other possible mass-to-surface ratios for the lightsail. The two panels show the maximum injection speed as a function of the deflection angle (left) and the travel time from Earth to α Cen AB as a function of time for an aluminum lattice sail as proposed by Drexler

(1979). The corresponding mass-to-surface ratio is $\sigma = 7 \times 10^{-2} \text{ gram m}^{-2}$. The results from these numerical simulations suggest that $v_{\infty, \text{max}}$ is about a factor of 10 smaller for any given deflection angle than for our nominal graphene-class sail and that the travel time is about a factor of 10 higher. This is consistent with our analytical estimate that $\tau \propto \sigma$ (see Equation 4), which suggests travel times of an aluminum lattice are extended by a factor of $\sqrt{7 \times 10^{-2} / 7.6 \times 10^{-4}} = 9.7$ compared to a graphene-class sail.

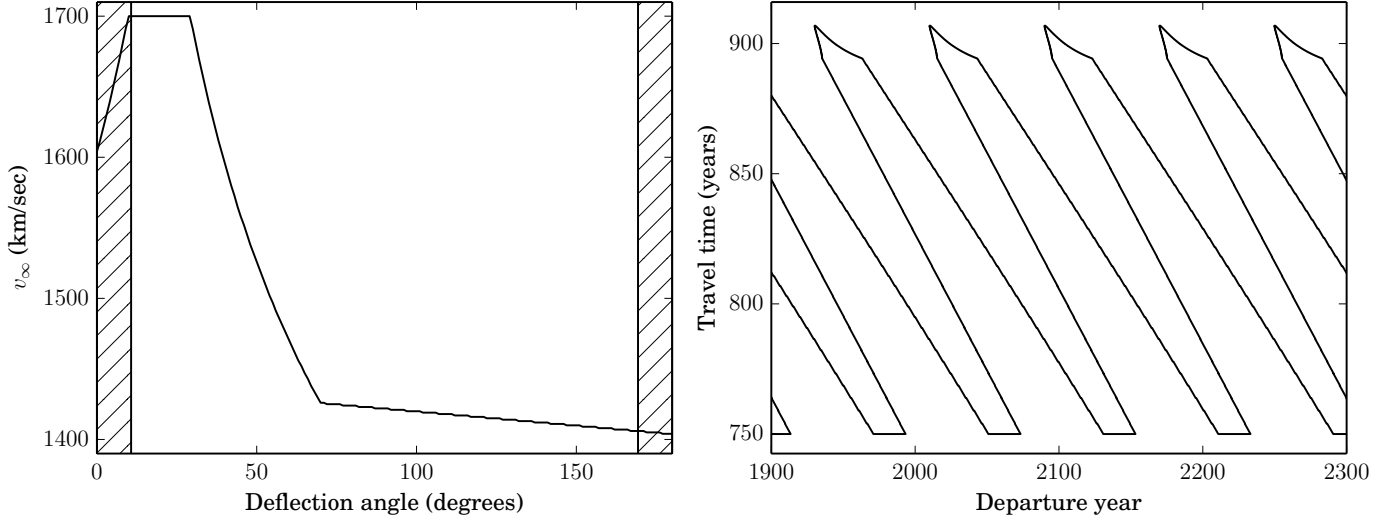


Figure 5. Same as top right and bottom left panels in Figure 4, but now for an aluminum lattice sail. The maximum injection velocities (left panel) are about a factor of 10 smaller for a given angle than in for the case of a graphene-class lightsail. Consequently, the corresponding travel times are a factor of 10 longer (right panel); see Equation (6).

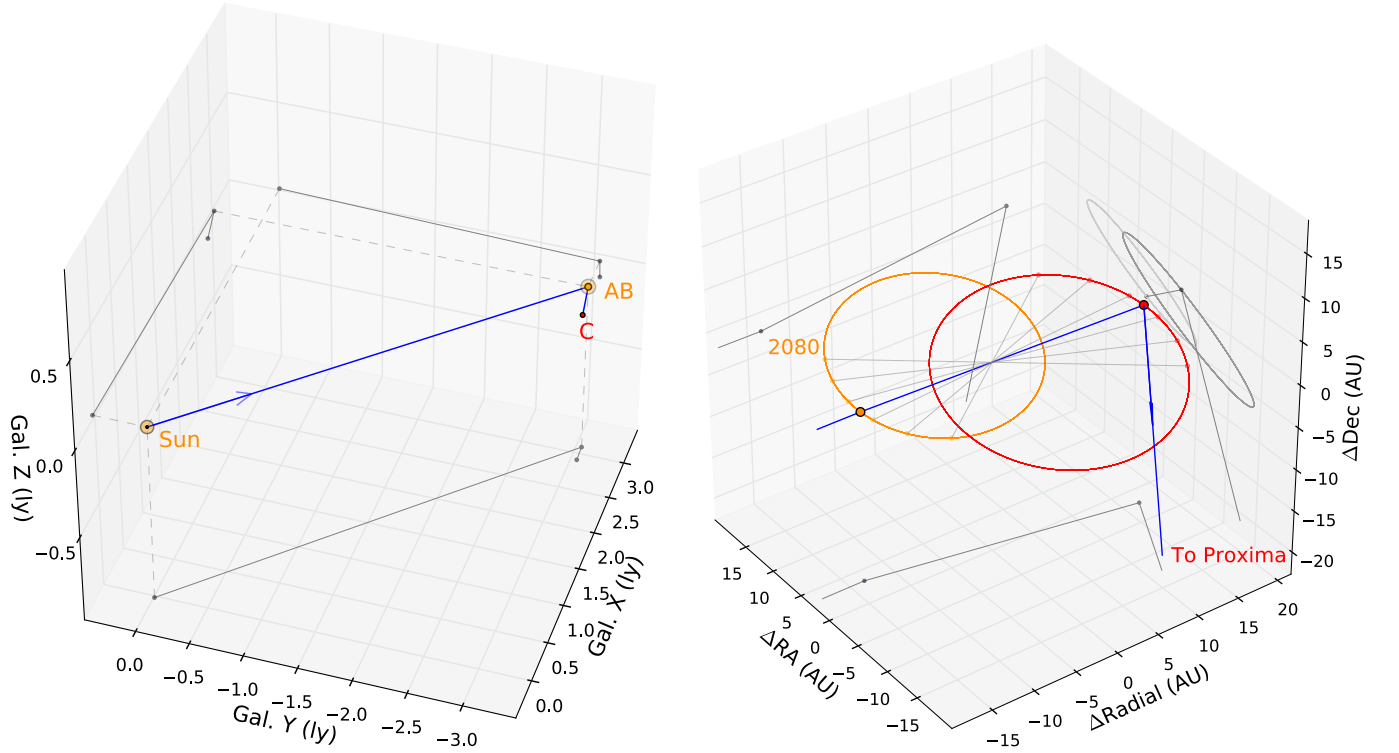


Figure 6. Example trajectory (blue line) of a lightsail from Earth performing photogravitational assists at α Cen A and B toward Proxima. Projections of the trajectory on the three planes of the coordinate systems are shown as gray lines. *Left:* Large-scale overview of the trajectory from the Sun to α Cen in Galactic coordinates (in units of ly). X increases toward the Galactic center, Y is positive toward the Galactic direction of rotation, and is Z positive toward the north Galactic pole. *Right:* Orbital configuration of the α Cen AB binary upon arrival of the lightsail in 2092.69. The origin of the differential cartesian ICRS coordinate system (in units of AU) is located in the α Cen AB barycenter. The points on the orbits of A (orange ellipse) and B (red ellipse) are separated by 5 yr to illustrate the evolution of the stellar positions. The projection of the binary orbit on the Earth sky is shown in the R.A.-decl. plane.

The right panel of Figure 5 covers times of departure from Earth between 1900 and 2300 as the bottom right panel of Figure 4. Minimum travel times for an aluminum-class lightsail are $750 \text{ yr} \lesssim \tau(t) \lesssim 910 \text{ yr}$. Note that any given departure year from Earth allows multiple, in fact, up to five possible travel times. Each individual travel time corresponds to a specific, sub- $v_{\infty, \text{max}}$ interstellar speed of the lightsail and a specific orbital cycle of the AB binary upon arrival.

Figure 6 illustrates the complete trajectory of a lightsail from Earth to α Cen A, B, and C with an arrival at α Cen AB in the year 2092.69. At that instance, the sky-projected AB separation is 19° and $v_{\infty, \text{max}} = 17,050 \text{ km s}^{-1}$ is possible, providing the minimum travel time from Earth of 75 yr (see Figure 4, bottom left). The left panel shows a global overview of the Sun-AB-C trajectory in Galactic coordinates and on a scale of light years. Our nominal graphene-class sail would require a minimum of 75 yr to cover the distance of the long blue line between the Sun and the AB binary and another 46 yr to complete the travel from the AB binary to C. The right panel shows a zoom into the AB binary at the time of arrival in 2092.69. With an instantaneous separation of 30.84 AU between A and B and assuming a residual speed of the sail of 8400 km s^{-1} (see Section 2.2.1), the travel time between encounters of A and B would be 6 days and 8.6 hours. After the encounter with B, the lightsail would be deflected toward Proxima. A projection of the blue trajectory on the Earth sky is shown in Figure 2.

3.2. Photogravitational Assists in the Solar Neighborhood

Moving on to other stars in the solar neighborhood, Figure 7 illustrates our findings for the minimum possible travel times of a graphene-class lightsail to perform a photogravitational assist to a full stop, i.e., into a bound orbit around the respective star. The left panel shows 117 stars within 21 ly, and the right panel shows 22,683 stars out to 316 ly. The meanings of the symbols and lines are described in the figure caption. For these full-stop maneuvers to work, note that the injection speeds need to be achieved at departure from the solar system in the first place.

As an intriguing result of this study, we find that Sirius A, though being about twice as far from the Sun as α Cen, could actually decelerate an incoming lightsail to a full stop after only about 69 yr of interstellar travel ($v_{\infty, \text{max}} = 12.5\% c$).³ This is due to the star’s particularly high luminosity of about 24.2 solar luminosities. The derived travel time compares to a minimum travel time of 75 yr to α Cen if a sequence of photogravitational

assists is used at stars A and B to perform a full stop, and it compares to 101 yr of interstellar travel to α Cen A or 148 yr to α Cen B if only the target star is used for a slowdown to zero. The case of Sirius is particularly interesting because it is actually a binary system and Sirius B is a white dwarf (Bessel 1844; Adams 1915). Photogravitational assists in the Sirius AB system would need an exact determination of the binary orbit prior to launch (for recent astrometry of the orbit, see Bond et al. 2017), which could then allow a sequence of flybys around an A1V main-sequence star and a white dwarf.

Table 2 lists our results for the maximum injection speeds and minimum travel durations to the 10 most nearby stars shown in Figure 7 in order to perform a full stop via photogravitational braking (the full list of 22,683 objects is available in the journal version of this article). The results have been obtained using numerical trajectory simulations from our modified N -body integrator. The objects are ordered by increasing travel time.

4. DISCUSSION

4.1. Launch Strategy and Aiming Accuracy

A graphene-class sail could have a maximum ejection speed of about $11,500 \text{ km s}^{-1}$ from the solar system if it was possible to bring it as close as five solar radii to the Sun and then initiate a photogravitational launch (Heller & Hippke 2017). This is much less than the maximum injection speed of $17,050 \text{ km s}^{-1}$ that can be absorbed by successive photogravitational assists at α Cen A to C. If sunlight were to be used to push a lightsail away from the solar system, then its propulsion would need to be supported by a second energy source, e.g. a ground-based laser array, to fully exploit the potential of photogravitational deceleration upon arrival. A combination with sunlight might in fact reduce the huge energy demands of a ground-based laser system.

The aiming accuracy at departure from the solar system is key to a successful photogravitational assist at α Cen. Hence, the position, proper motion, and the binary orbital motion of the α Cen AB binary will need to be known very precisely at the time of departure. This is a rather delicate question as Gaia will not observe α Cen AB at all.

The angular diameter of α Cen A is about $0.008'' = 8 \text{ mas}$ as seen from Earth (Kervella et al. 2003, 2017a). In order for an interstellar projectile to successfully hit α Cen A, a pointing accuracy of $< R_\star$ is key. A fiducial accuracy of $0.2 R_\star$ translates into a funnel $< 1.6 \text{ mas}$ as seen from Earth. The current uncertainty of 3.9 mas yr^{-1} in the proper motion (pm) vector of α Cen ($\mu = 3685.8 \pm 3.9 \text{ mas/yr}$; Kervella et al. 2016) will result in an offset of 78 mas (0.1 AU at α Cen) after a nominal 20 yr journey, as proposed by the Breakthrough Starshot Initiative. Hence, the current knowledge of the celestial position and motion of α Cen AB prevents an aimed orbital injection and swing-by to Proxima. That said, pm

³ Heller & Hippke (2017) calculated a value of $v_{\infty, \text{max}} = 14.9\% c$. They used $r_{\text{min}} = 5 R_\star$ without any constraints on the maximum effective temperature of the sail to prevent overheating, see Equation (10).

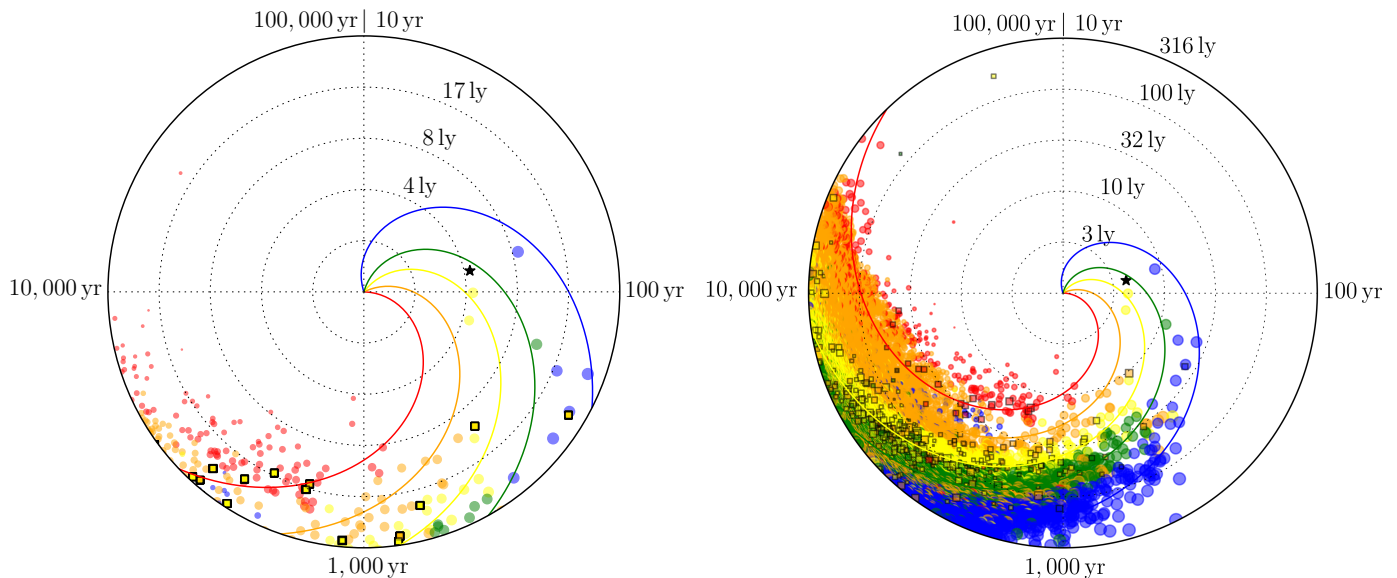


Figure 7. Travel times (hour angles) versus stellar distance to the solar system (radial coordinate) for stars in the solar neighborhood. Symbols refer to numerical trajectory simulations to individual targets; lines illustrate logarithmic spirals as per Equation (6) for $r_{\min} = 5 R_{\star}$. These spirals are parameterized using M2V (red), K5V (orange), G2V (yellow), F3V (green), and A0V (blue) template stars (Pecaut & Mamajek 2013). Square symbols depict stars with known exoplanets. The black star symbol denotes α Cen. *Left:* All 117 stars within 21 ly around the Sun. *Right:* 22,683 stars out to 316 ly around the Sun.

Table 2. An Interstellar Travel Catalog to Use Photogravitational Assists for a Full Stop.

#	Name	Travel time (yr)	Distance (ly)	Luminosity (L_{\odot})	Maximum injection speed (km s^{-1})
1.	Sirius A ^a	68.90	8.58	24.20	37,359
2.	α Centauri A ^b	101.25	4.36	1.56	12,919
3.	α Centauri B ^b	147.58	4.36	0.56	8863
4.	Procyon A ^a	154.06	11.44	6.94	22,278
5.	Altair	176.67	16.69	10.70	28,341
6.	Fomalhaut A ^c	221.33	25.13	16.67	34,062
7.	Vega	262.80	25.30	37.0	28,883
8.	Epsilon Eridiani	363.35	10.50	0.495	8669
9.	Rasalhague	364.9	46.2	25.81	37,977
10.	Arcturus	369.4	36.7	170	29,806

^aHost to a white dwarf companion.

^bSuccessive assists at α Cen A and B could allow deceleration from much faster injection speeds, reducing travel times to 75 yr to both stars (see Section 3.1).

^cHost to an exoplanet, a debris disk, and two companion stars, one of which shows an accretion disk itself.

NOTE—Stars are ordered by increasing travel time from Earth. The hypothetical lightsail has a nominal mass-to-surface ratio (σ_{nom}) of $8.6 \times 10^{-4} \text{ gram m}^{-2}$. Travel times for different σ values scale as $\sqrt{\sigma/\sigma_{\text{nom}}}$. The full list of 22,683 objects is available in the journal version of this article.

accuracies $< 2 \text{ mas}/20 \text{ yr} = 100 \mu\text{as yr}^{-1}$ can in principle

be reached for α Cen using dedicated astrometry. These

observations will be key to a successful direction of an interstellar ballistic probe from Earth to α Cen.

The aiming accuracy will also be affected by the presence of interstellar magnetic fields if the sail has an electric charge. In fact, it might be impossible for a sail to prevent getting electrically charged due to the continuous collisions with the interstellar medium. Studies of the effects of magnetic effects on the interstellar trajectories of lightsails are beyond the scope of this study but they might be crucial to assess whether aiming accuracies of the order of one stellar radius at the target are actually possible.

4.2. Deflection during Stellar Encounter

The limiting factor to the full leverage of the additive nature of the photogravitational effect in the α Cen AB system is in their orbital inclination with respect to the Earth’s line of sight. The optimal deflection angle to achieve maximum injection speeds at α Cen A is 19° (Figure 4). A and B will never come closer than 10.7° from our point of view. If it were possible to let the incoming lightsail tack from an angle (λ), or “from the side”, then this might allow faster departures than permitted for straight trajectories if the sky-projected AB angular separation upon arrival is $> 19^\circ$ (see Figure 4, top right). In fact, due to the binary’s sky-projected proper motion of 23.4 km s^{-1} and given α Cen A’s barycentric tangential velocity of $\approx 8 \pm 5 \text{ km s}^{-1}$ (Kervella et al. 2016) upon encounter, the incoming sail will have a minimal ($\approx 0.1^\circ$) tangential velocity with respect to the line of sight from Earth.

We have looked at different possibilities to add an additional tangential speed component (v_x) to the sail and found that $\lambda = \arctan(v_x/v_\infty)$. One option that seems physically feasible, though technically challenging, would be to send the sail with a slight offset to α Cen A, and then fire the onboard communication laser perpendicular to the trajectory for a time t_1 . This maneuver would result in a curved sail trajectory. Assuming that the laser energy output ($E_1 = P_1 t_1$; P_1 being the laser power) would be transformed into kinetic energy of the sail (E_{kin}), we have

$$\lambda = \arctan(v_x/v_\infty) = \arctan\left(\sqrt{\frac{2P_1 t_1}{M}} v_\infty^{-1}\right). \quad (12)$$

To deflect our fiducial sail with $v_\infty = 17,050 \text{ km s}^{-1}$ by $\lambda = 1^\circ$, a 100 W (or a 10 kW) laser would have to fire for a whole year (or 10 days), yielding $E_1 = 8.6 \times 10^9 \text{ GJ}$. If an adequate miniature propulsion system could be implemented to change the incoming trajectory by 1° , then the gain in $v_{\infty, \text{max}}$ would be up to several 100 km s^{-1} and the travel time from Earth to α Cen A could be reduced by a few years.

Assuming that this maneuver shall not add more than about one gram to the total weight, we find that an

energy density of $8.6 \times 10^9 \text{ GJ/gram}$ is several orders of magnitudes higher than that of conventional chemical reactants or of modern lithium batteries. Only nuclear fission could possibly yield high enough energy densities, but this technology would likely add up to much more weight to feed the laser. In turn, an increased weight will reduce the tangential velocity that can be achieved through the conversion of laser power into kinetic energy. We conclude that current means of energy storage and conversion do not permit higher incoming sail speeds $v_{\infty, \text{max}}$ by steering the sail onto a significantly curved trajectory.

4.3. Sirius Afterburner

Using numerical simulations, we investigated scenarios in which a graphene-class lightsail approaches Sirius A from Earth but minimizing the deceleration during approach while maximizing the acceleration after passage of r_{min} (set to $5.64 R_\star$ to prevent fatal damage). We refer to this setup as the “Sirius afterburner” since the star is used to accelerate the space probe to even faster interstellar velocities than might be achievable with Earth-based technology and/or using solar photons.

We find that such a flyby at Sirius A can increase the velocity of a graphene-class lightsail by up to $27,000 \text{ km s}^{-1}$ ($9.0\% c$) in the non-relativistic regime with deflection angles $\delta \lesssim 20^\circ$. Consequently, stars at distances $d_\star > d_S$ to the Sun (d_S being the Sun–Sirius distance) and within a sky-projected angle

$$\varphi = \delta \left(1 - \arcsin\left(\frac{d_S}{d_\star}\right)\right) \quad (13)$$

around Sirius (as seen from Earth) can be reached significantly faster using a photogravitational assist at Sirius. The maximum velocity boost of $9.0\% c$ is smaller than $v_{\infty, \text{max}} = 12.5\% c$, which we determined as the maximum loss of speed upon arrival at Sirius A to a full stop in Section 3.2, as the stellar photon pressure is not acting antiparallel to the instantaneous velocity vector during flyby.

The same principle applies to other combinations of nearby and background stars, but Sirius A with its huge luminosity and relative proximity to the Sun is the most natural choice for an interstellar photogravitational hub for humanity.

4.4. Particular Objects to Visit in the Solar Neighborhood

Beyond the many single-target stars, there are other interesting objects in the solar neighborhood, which an ultralight photon sail could approach into a bound orbit after deceleration at the host star, such as

1. The nearby exoplanet Proxima b (Anglada-Escudé et al. 2016);

2. A total of 328 known exoplanet host stars within 316 ly (right panel Figure 7);
3. The young Fomalhaut triple system with its enigmatic exoplanet Fomalhaut b (Kalas et al. 2008) and protoplanetary debris disks around Fomalhaut A and C (Holland et al. 1998; Kennedy et al. 2014);
4. The two white dwarfs Sirius B, located at 8.6 ly from the Sun, and Procyon B at a distance of 11.44 ly;
5. 36 Ophiuchi, consisting of three K stars and located at 19.5 ly from the Sun, is the most nearby stellar triple;
6. TV Crateris, a quadruple system of T Tauri stars and located at 150 ly from the Sun; and
7. PSR J0108-1431, between about 280 ly and 424 ly away, is the nearest neutron star (Tauris et al. 1994).

Fomalhaut A is a moderately fast rotator with rotational speeds of about 100 km s^{-1} at the equator. Altair and Vega are very fast rotating stars (Aufdenberg et al. 2006) with strongly anisotropic radiation fields. This would certainly affect the steering of the sail. An interstellar probe from Earth would approach Vega from a polar perspective. With the poles being much hotter and thus more luminous than the rest of the star, this could be beneficial for an efficient braking.

Beyond that, it could be possible to visit stars of almost any spectral type from red dwarf stars to giant early-type stars, which would allow studies of stellar physics on a fundamentally new level of detail. In principle, an adaptation of the Breakthrough Starshot concept that is capable of flying photogravitational assists could visit these objects and conduct observations from a nearby orbit. That said, photogravitational assists into bound orbits around single low-luminous M dwarfs imply very long travel times even in the solar neighborhood. The case of Proxima and its habitable zone exoplanet Proxima b is an exceptional case since this red dwarf is a companion of two Sun-like stars, both of which can be used as photon bumpers to allow a fast and relatively short travel to Proxima.

4.5. Prospects of Building a Highly Reflective Graphene Sail

Since the advent of modern graphene studies in the early 2000s (Novoselov et al. 2004)⁴, huge progress has been made in the characterization of this material and in

its high-quality, wafer-scale production (Lee et al. 2014). For example, Sanchez-Valencia et al. (2014) presented a method to synthesize single-walled carbon nanotubes, which have interesting electronic properties that make it a candidate material for extremely light wires in the onboard electronics of a graphene-class sail. Carbon nanotubes might also be the natural choice for a material to build a rigid sail skeleton of. Sorensen et al. (2016) patented a high-yield method for the gram-scale production of pristine graphene nanosheets through a controlled, catalyst-free detonation of C_2H_2 in the presence of O_2 .

Private companies offer cm^2 -sized mono-atomic layers of graphene sheets at a price of about 75 EUR, which translates into a price of 750 million EUR for a 10^5 m^2 sail. If the price decline for graphene production continues its trend of three orders of magnitude per decade over the next 10 years, this could result in costs of 750,000 EUR for the production of graphene required for a 10^5 m^2 sail in the late 2020s. The availability of affordable, high-quality graphene for large structures is key to the mission concept assumed in this study. It might be necessary to send several probes for the purpose of redundancy to ensure that at least one sail out of a fleet will survive decades of interstellar travel and successfully perform the close stellar encounters.

One key challenge that will affect the sail's performance of a photogravity assist is in the emergence of inhomogeneities of the reflectivity across the sail area. A sail reflectivity of 99.99% has been assumed in our calculations, but the bombardment of the interstellar medium will create tiny holes in the sail (Hoang et al. 2017) that would cause local decreases of reflectivity. Certainly, the sail would need to be able to autonomously compensate for the resulting torques during the deceleration phase, e.g. via proper orientation with respect to the approaching star.

5. CONCLUSION

This report describes a new means of using stellar photons, e.g. in the α Cen system, to decelerate and deflect an incoming ultralight photon sail from Earth. This improved method of using photogravitational assists is different from gravitational slingshots as they have been performed many times in the solar system and different from the photogravitational assists described by Heller & Hippke (2017), in the sense that the lightsail is not flung around the star but it rather passes in front of it. In other words, we propose that the star is not being used as a catapult but rather as a bumper. If the mass-to-surface ratio of the lightsail is sufficiently small, then photogravitational assists may absorb enough kinetic energy to park it in a bound circumstellar orbit or even transfer it to other stellar or planetary members in the system.

Proxima b, the closest extrasolar planet to us, is a natural prime target for such an interstellar lightsail.

⁴ Awarded with "The Nobel Prize in Physics 2010". Nobel-prize.org. Nobel Media AB 2014. Web. 5 April 2017. http://www.nobelprize.org/nobel_prizes/physics/laureates/2010

Its M dwarf host star has a very low luminosity that could only absorb small amounts of kinetic energy from an incoming lightsail. Its two companion stars α Cen A and B, however, have roughly Sun-like luminosities, which means that successive photogravitational assists at α Cen A, B, and Proxima could be sufficiently effective to bring an ultralight photon sail to rest.

In this paper, we investigate the case of a graphene-class sail with a nominal mass-to-surface ratio of $\sigma_{\text{nom}} = 8.6 \times 10^{-4} \text{ gram m}^{-2}$ and find that our improved “bumper” technique of using photogravitational assists allows maximum injection speeds of up to $v_{\infty, \text{max}} = 17,050 \text{ km s}^{-1}$ (5.7% c) at α Cen A, implying travel times as short as 75 yr from Earth. The maximum injection speed at Proxima is 1270 km s^{-1} , which the sail would be left with after assists at α Cen A and B. This residual speed means another 46 yr of travel between the AB binary and Proxima, or a total of 121 yr from Earth. Travel times for lightsails with larger mass-to-surface ratios (σ) scale as $\sqrt{\sigma/\sigma_{\text{nom}}}$.

The exact value of $v_{\infty, \text{max}}$ at the α Cen system depends on the deflection angle (δ) required by the sail to go from A to B and, hence, $v_{\infty, \text{max}}$ depends on the instantaneous orbital alignment of the AB binary upon arrival of the sail. We performed numerical simulations of sail trajectories under the effects of both the gravitational forces between the sail and the star and the stellar photon pressure acting upon the sail to parameterize $v_{\infty, \text{max}}(\delta)$. We then used calculations of the orbital motions of the AB stars to first obtain $\delta(t)$ and then $v_{\infty, \text{max}}(t)$ for the next 300 yr. This provides us with the expected travel times $\tau(t)$ and with the times of arrival at α Cen A for launches within the next 300 yr. In general, we find that $75 \text{ yr} \leq \tau(t) \leq 95 \text{ yr}$ for a graphene-class sail cruising with $v_{\infty, \text{max}}$.

A minimum in the travel time, which might be interesting for real mission planning, occurs for a departure on 8 September 2092 with a photogravitational assist at α Cen A in late 2167 after 75 yr of interstellar travel. The difference between the maximum and minimum travel times to permit photogravitational assists from α Cen A via B to Proxima is only about 20 yr, so that an earlier departure (e.g. in 2040) might entail somewhat longer travel times (e.g. 91 yr) but still allow a much earlier arrival (e.g. 2131) than the departure near the next minimum of $\tau(t)$.

Beyond that, photogravitational assists may allow injections into bound orbits around other nearby stars

within relatively short travel times. We identified Sirius A as the star that permits the shortest travel times for a lightsail using stellar photons to decelerate into a bound orbit. At a distance of about 8.6 ly, it is almost twice as distant as the α Cen system, but its huge power output of about 24 solar luminosities allows injection speeds of up to $v_{\infty, \text{max}} = 37,300 \text{ km s}^{-1}$ (12.5% c). These speeds cannot be obtained from the solar photons alone upon departure from the solar system, and so additional technologies (e.g. a ground-based laser array) will need to be used to accelerate the sail to the maximum injection speed at Sirius A. Beyond the compelling opportunity of sending an interstellar spacecraft into a bound orbit around Sirius A within a human lifetime, its white dwarf companion Sirius B could be visited as well using a photogravitational assist at Sirius A. We identify other interesting targets in the solar neighborhood that allow photogravitational assists into bound orbits, the first 10 of which imply travel times between about 75 yr (α Cen AB) and 360 yr (Epsilon Eridiani) with a nominal graphene-class lightsail.

Many of the technological components of the lightsail envisioned in this study are already available, e.g. conventional spacecraft to bring the lightsails into near-Earth orbits for sun- or laser-assisted departure. Other components are currently being developed, e.g. procedures for the large-scale production of graphene sheets, nanowires with the necessary electronic properties consisting of single carbon atom layers, gram-scale cameras and lasers (for communication between the sail and Earth), or sub-gram-scale computer chips required to perform onboard processing etc. We thus expect that a concerted effort of electronic, nano-scale, and space industries and research consortia could permit the construction and launch of ultralight photon sails capable of interstellar travels and photogravitational assists, e.g. to Proxima b, within the next few decades.

The authors thank an anonymous referee for her or his valuable report. This work was supported in part by the German space agency (Deutsches Zentrum für Luft- und Raumfahrt) under PLATO Data Center grant 500O1501 and it made use of NASA’s Astrophysics Data System Bibliographic Services. This work has made use of data from the European Space Agency (ESA) mission *Gaia* (<https://www.cosmos.esa.int/gaia>), processed by the *Gaia* Data Processing and Analysis Consortium (DPAC; <https://www.cosmos.esa.int/web/gaia/dpac/consortium>).

REFERENCES

- Adams, W. S. 1915, *PASP*, 27, 236
- Allende Prieto, C., Barklem, P. S., Lambert, D. L., & Cunha, K. 2004, *A&A*, 420, 183
- Anglada-Escudé, G., Amado, P. J., Barnes, J., et al. 2016, *Nature*, 536, 437
- Aufdenberg, J. P., Mérand, A., Coudé du Foresto, V., et al. 2006, *ApJ*, 645, 664

- Bessel, F. W. 1844, *MNRAS*, **6**, 136
- Bond, H. E., Schaefer, G. H., Gilliland, R. L., et al. 2017, *ApJ*, **840**, 70
- Casey, A. R., Hawkins, K., Hogg, D. W., et al. 2017, *ApJ*, **840**, 59
- Cester, B., Ferluga, S., & Boehm, C. 1983, *Ap&SS*, **96**, 125
- Dachwald, B. 2005, *Journal of Guidance, Control, and Dynamics*, **28**, 1187
- Drexler, K. 1979, Design of a High Performance Solar Sail System, SSL report (Space Systems Laboratory, Department of Aeronautics and Astronautics, Massachusetts Institute of Technology)
- Forward, R. L. 1962, *Missiles and Rockets*, **10**, 26
- Gaia Collaboration, Brown, A. G. A., Vallenari, A., et al. 2016a, *A&A*, **595**, A2
- Gaia Collaboration, Prusti, T., de Bruijne, J. H. J., et al. 2016b, *A&A*, **595**, A1
- Garwin, R. L. 1958, *Jet Propulsion*, **28**, 188
- Heller, R., & Hippke, M. 2017, *ApJL*, **835**, L32
- Heller, R., Mislis, D., & Antoniadis, J. 2009, *A&A*, **508**, 1509
- Hoang, T., Lazarian, A., Burkhart, B., & Loeb, A. 2017, *ApJ*, **837**, 5
- Høg, E., Fabricius, C., Makarov, V. V., et al. 2000, *A&A*, **355**, L27
- Holland, W. S., Greaves, J. S., Zuckerman, B., et al. 1998, *Nature*, **392**, 788
- Holmberg, J., Nordström, B., & Andersen, J. 2009, *A&A*, **501**, 941
- Intel Corporation. 2016, Intel®Xeon®Processor E5 v4 Product Family – Thermal Mechanical Specification and Design Guide, Intel Corporation, 2200 Mission College Blvd., Santa Clara, CA 95054-1549, USA
- Kalas, P., Graham, J. R., Chiang, E., et al. 2008, *Science*, **322**, 1345
- Kennedy, G. M., Wyatt, M. C., Kalas, P., et al. 2014, *MNRAS*, **438**, L96
- Kepler, J. 1619, De cometis libelli tres I. astronomicus, theoremata continens de novam ... III. astrologicus, de significationibus cometarum annorum motu cometarum ... II. physicus, continens physiologiam cometarum 1607 et 1618
- Kervella, P., Bigot, L., Gallenne, A., & Thévenin, F. 2017a, *A&A*, **597**, A137
- Kervella, P., Mignard, F., Mérand, A., & Thévenin, F. 2016, *A&A*, **594**, A107
- Kervella, P., Thévenin, F., & Lovis, C. 2017b, *A&A*, **598**, L7
- Kervella, P., Thévenin, F., Ségransan, D., et al. 2003, *A&A*, **404**, 1087
- Kunder, A., Kordopatis, G., Steinmetz, M., et al. 2017, *AJ*, **153**, 75
- Lee, J.-H., Lee, E. K., Joo, W.-J., et al. 2014, *Science*, **344**, 286
- Lindgren, L., Lammers, U., Bastian, U., et al. 2016, *A&A*, **595**, A4
- Liu, Z., Liu, X., Wang, Y., & Pan, P. 2016, *Journal of Physics D Applied Physics*, **49**, 195101
- Los, J. H., Zakharchenko, K. V., Katsnelson, M. I., & Fasolino, A. 2015, *PhRvB*, **91**, 045415
- Lubin, P. 2016, *Journal of the British Interplanetary Society*, **69**, 40
- Manchester, Z., & Loeb, A. 2017, *ApJL*, **837**, L20
- Marx, G. 1966, *Nature*, **211**, 22
- Matloff, G. L. 2013, *Journal of the British Interplanetary Society*, **66**, 377
- Matloff, G. L., Kezerashvili, R. Y., Maccone, C., & Johnson, L. 2008, ArXiv e-prints, [arXiv:0809.3535](https://arxiv.org/abs/0809.3535) [[physics.space-ph](https://arxiv.org/abs/0809.3535)]
- McInnes, C. R., & Brown, J. C. 1990, *Celestial Mechanics and Dynamical Astronomy*, **49**, 249
- Moitra, P., Slovick, B. A., Gang Yu, Z., Krishnamurthy, S., & Valentine, J. 2014, *Applied Physics Letters*, **104**, 171102
- Moitra, P., Slovick, B. A., Yu, Z. G., Krishnamurthy, S., & Valentine, J. 2014, *Applied Physics Letters*, **104**, 171102
- Novoselov, K. S., Geim, A. K., Morozov, S. V., et al. 2004, *Science*, **306**, 666
- Pecaut, M. J., & Mamajek, E. E. 2013, *ApJS*, **208**, 9
- Perryman, M. A. C., Lindgren, L., Kovalevsky, J., et al. 1997, *A&A*, **323**, L49
- Redding, J. L. 1967, *Nature*, **213**, 588
- Ridenoure, R. W., Munakta, R., Wong, S. D., et al. 2016, *Journal of Small Satellites*, **5**, 531
- Sanchez-Valencia, J. R., Diemel, T., Groning, O., et al. 2014, *Nature*, **512**, 61
- Slovick, B., Yu, Z. G., Berding, M., & Krishnamurthy, S. 2013, *Phys. Rev. B*, **88**, 165116
- Slovick, B., Yu, Z. G., Berding, M., & Krishnamurthy, S. 2013, *PhRvB*, **88**, 165116
- Sorensen, C., Nepal, A., & Singh, G. 2016, Process for high-yield production of graphene via detonation of carbon-containing material, uS Patent 9,440,857
- Tauris, T. M., Nicastro, L., Johnston, S., et al. 1994, *ApJL*, **428**, L53
- Tsander, K. 1924, NASA Technical Translation TTF-541
- Tsiolkovskiy, K. E. 1936, United Scientific and Technical Presses (NIT), 2
- Tsu, T. C. 1959, *ARS Journal*, **29**, 442

Tsuda, Y., Mori, O., Funase, R., et al. 2011, *Acta Astronautica*, 69, 833

Valenti, J. A., & Fischer, D. A. 2005, *ApJS*, 159, 141
van Leeuwen, F. 2007, *A&A*, 474, 653